Relativistic many-body calculations of excitation energies, line strengths, transition rates, and oscillator strengths in Pd-like ions

U.I. Safronova* and T. E. Cowan
Physics Department, University of Nevada, Reno, NV 89557

W. R. Johnson†
Department of Physics, University of Notre Dame, Notre Dame, IN 46566

(Dated: March 3, 2005)

Excitation energies, line strengths, oscillator strengths, and transition probabilities are calculated for $4d^{-1}4f$, $4d^{-1}5p$, $4d^{-1}5f$, and $4d^{-1}6p$ hole-particle states in Pd-like ions with nuclear charges Z ranging from 49 to 100. Relativistic many-body perturbation theory (MBPT), including the Breit interaction, is used to evaluate retarded E1 matrix elements in length and velocity forms. The calculations start from a [Kr]$4d^{10}$ closed-shell Dirac-Hartree-Fock (DHF) potential and include second- and third-order Coulomb corrections and second-order Breit-Coulomb corrections. First-order perturbation theory is used to obtain intermediate-coupling coefficients and second-order MBPT is used to determine matrix elements. Contributions from negative-energy states are included in the second-order electric-dipole matrix elements. The resulting transition energies, line strengths, and transition rates are compared with experimental values and with other recent calculations. Trends of oscillator strengths as functions of nuclear charge Z are shown graphically for all transitions from the $4d^{-1}4f$, $4d^{-1}5p$, $4d^{-1}5f$, and $4d^{-1}6p$ states to the ground state.

PACS numbers: 31.15.Ar, 31.15.Md, 32.70.Cs, 32.30.Rj, 31.25.Jf

I. INTRODUCTION

Relativistic MBPT studies of hole-particle excitations of closed-shell ions were performed by Avgoustoglou et al. [1–4] for Ne-like ions and by Safronova et al. [5, 6] for Ne- and Ni-like ions. The ground states of Ne-like and Ni-like ions have completely filled n=1, 2 and n=1, 2, 3 shells, respectively, whereas the ground states of Pd-like ions have closed $4s$, $4p$, and $4d$ subshells and an open $4f$ subshell. In Fig. 1, we plot one-electron DHF energies of $4f$ and $5p$ states as functions of Z. As one can see from this figure, the $5p$ orbitals are more tightly bound than the $4f$ orbitals at low stages of ionization while $4f$ orbitals are more tightly bound for highly ionized cases. Competition between $4f$ and $5p$ orbitals leads to problems for MBPT, making it difficult to obtain very accurate excitation energies and line strengths for the transition between the low lying $4d^9 4f$, $4d^9 5p$, $4d^9 5f$, and $4d^9 6p$ excited states and the ground state.

Earlier line strength calculations for the $4d^{10}\,{}^1S$ - $4d^9 4f\,{}^1P$ resonance transition along the palladium isoelectronic sequence were performed Younger [7] in three approximations: configuration-averaged HF, term-dependent HF, and MBPT. Numerical results were given in [7] for three Pd-like ions, Xe^{+8}, Nd^{14+}, and W^{+28}. Relative magnitudes of electric-multipole (E1, E2, E3) and magnetic-multipole (M1, M2, M3) radiative decay rates, calculated using the multi-configuration DHF approach, were presented by Biémont [8] for the $4d^9 4f$, $4d^9 5s$, and $4d^9 5p$ states of highly ionized Pd-like ions.

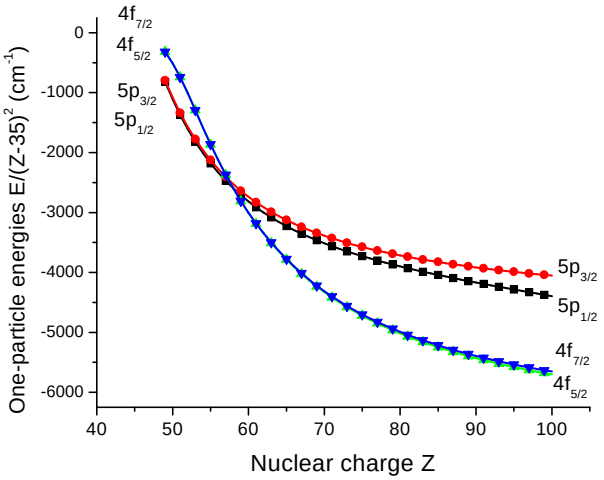

FIG. 1: One-electron DHF energies ($E/(Z-35)^2$ in cm^{-1}) of $4f_j$ and $5p_j$ states as functions of Z.

Sugar and Kaufman [9] extended the identification of resonance lines of $4d^9 4f$ and $4d^9 5p$ configurations in the Pd I isoelectronic sequence from Nd^{+14} to Ho^{+21}. Spectra were obtained with a high voltage spark and photographed with 10.7 m grazing incidence spectrograph. Calculations of energy levels and eigenvectors were also made in Ref. [9], including configuration interaction between $4d^9 4f$ and $4d^9 5p$ using scaled HF values for radial integrals. A review of all previous identifications of resonance lines of the $4d^9 4f$ and $4d^9 5p$ configurations

*Electronic address: usafrono@nd.edu
†Electronic address: johnson@nd.edu; URL: www.nd.edu/~johnson

was also given in [9]. Spectra of highly ionized Er, Yb, Hf, W, and Pt were observed by Sugar and Kaufman [10] by injecting these elements into the plasma of the TEXT tokamak at the University of Texas at Austin. Resonance lines of the $4d^{10}$–$4d^9 4f$ transition array in Pd-like ions were identified in [10] by comparison with plots of observed-minus-calculated transition energies. A detailed analysis of various transitions in Pd-like ions was performed by Churlikov et al. [11–15]. To predict the $4d^{10}$ - $4d^9(np+n'f)$ transitions in Cd III–Cs X, relativistic HF calculations using the Cowan code with scaling were carried out in Ref. [11]. The $4d^9 5l$–$4d^9 5l'$ spectra in Pd-like ions Sb VI, Te VII, and I VIII were investigated in the 400–900 Åregion using vacuum spark sources in Ref. [12]. Experimental results for $4d^9 5s$, $4d^9 5d$, and $4d^9 5p$ states in Cs X–Ce XIII ions were obtained in Ref. [14] with the aid of high resolution spectrographs supplemented by theoretical calculations made using the Cowan code and by fitting with orthogonal operator techniques. It was emphasized in [14] that ions of the palladium isoelectronic sequence are currently interesting for the development of extreme-ultraviolet (XUV) lasers. High-resolution spectra of xenon ions from Xe IX to Xe XIV at 95–155 Å were presented in Churilov et al. [15]. In the region of importance for XUV lithography (near 134 Å) the strongest lines were identified as $4d^8$–$4d^7 5p$ transitions in Xe XI. The most intense lines in Xe IX were found to be the $4d^{10}\,{}^1S_0$–$4d^9 4f\,{}^1P_1$ line at 120.135 Å and the $4d^{10}\,{}^1S_0$–$4d^9 4f\,{}^3D_1$ line at 143.614 Å.

In the present paper, relativistic many-body perturbation theory is used to determine energies of Pd-like ions. Second-order MBPT calculations for Pd-like ions start from a $4d^{10}$ DHF potential. Third-order one-body Coulomb contributions are also included in the present calculation and found to significantly improve the agreement between calculation and measurement. We consider $4d$ holes and $4f$, $5p$, $5f$, and $6p$ particles leading to 12 odd-parity $4d^{-1}nl'[J]$ states with J=1. We calculate energies of these 12 states for ions with nuclear charge Z = 49 - 100.

Relativistic MBPT is also used to determine reduced matrix elements, line strengths, oscillator strengths, and transition rates for electric dipole transitions from the $4d^9 nl'$ states to the $4d^{10}\,{}^1S_0$ ground state in Pd-like ions. Retarded E1 matrix elements are evaluated in both length and velocity forms. The MBPT calculations start from a nonlocal $4d^{10}$ DHF potential and consequently give gauge-dependent transition matrix elements. Second-order correlation corrections compensate almost exactly for the gauge dependence of the first-order matrix elements, leading to corrected matrix elements that differ by less than 5% in length and velocity forms throughout the isoelectronic sequence. A detailed breakdown of contributions to energies and transition matrix elements for the case of $Xe^{+8}$is given in Appendices A and B, respectively.

TABLE I: J=1 hole-particle states in the $4djnl'j'$ complex for Pd-like ions in jj and LS coupling schemes.

jj	LS	jj	LS
$4d_{5/2}5p_{3/2}[1]$	$4d5p\,{}^3P_1$	$4d_{5/2}6p_{3/2}[1]$	$4d6p\,{}^3P_1$
$4d_{3/2}5p_{1/2}[1]$	$4d5p\,{}^1P_1$	$4d_{3/2}6p_{1/2}[1]$	$4d6p\,{}^1P_1$
$4d_{3/2}5p_{3/2}[1]$	$4d5p\,{}^3D_1$	$4d_{3/2}6p_{3/2}[1]$	$4d6p\,{}^3D_1$
$4d_{5/2}4f_{5/2}[1]$	$4d4f\,{}^3P_1$	$4d_{5/2}5f_{5/2}[1]$	$4d5f\,{}^3P_1$
$4d_{5/2}4f_{7/2}[1]$	$4d4f\,{}^3D_1$	$4d_{5/2}5f_{7/2}[1]$	$4d5f\,{}^3D_1$
$4d_{3/2}4f_{5/2}[1]$	$4d4f\,{}^1P_1$	$4d_{3/2}5f_{5/2}[1]$	$4d5f\,{}^1P_1$

II. SECOND-ORDER MBPT CALCULATIONS OF ENERGIES OF PD-LIKE IONS

Details of the MBPT method were presented in [1, 6] for calculation of energies of hole-particle states, in [16] for calculation of energies of particle-particle states, in [17] for calculation of radiative electric-dipole rates in two-particle states, and in [5] for calculation of multipole radiative rates in Ne-like systems. Here, we present only the model space for Pd-like ions without repeating the detailed discussions given in Refs. [1, 5, 6, 16, 17]. Differences between the calculations for Ni- and Pd-like ions arise because of the increased number of the core orbitals in the DHF potential ($1s^2 2s^2 2p^6 3s^2 3p^6 3d^{10} 4s^2 4p^6 4d^{10}$ instead of $1s^2 2s^2 2p^6 3s^2 3p^6 3d^{10}$) and the strong mixing between odd-parity states ($4d^{-1}4f + 4d^{-1}5p$). These differences lead to much more laborious numerical calculations. The calculations are carried out using finite basis set DHF orbitals. The orbitals used in the present calculation are obtained as linear combinations of B-splines. The B-spline basis orbitals are calculated using the method described in Ref. [18]. We use 40 B-splines of order 7 for each single-particle angular momentum state and we include all orbitals with orbital angular momentum $l \leq 9$ in our basis.

A. Model space

For atoms with one hole in closed shells and one particle above closed shells, the model space is formed from hole-particle states of the type $a_v^\dagger a_a|0\rangle$, where $|0\rangle$ is the $[\mathrm{Kr}]4d_{3/2}^4 4d_{5/2}^6$ ground state. The operators a_a and $a_v^\dagger$ are core annihilation and particle creation operators, respectively. Particle indices v range over states in the valence shell and hole indices a range over the closed core. In our study of low-lying $4d^{-1}nl$ states of Pd-like ions, values of a are limited to $4d_{3/2}$ and $4d_{5/2}$, while values of v are $4f_{5/2}$, $4f_{7/2}$, $5p_{1/2}$, $5p_{3/2}$, $5f_{5/2}$, $5f_{7/2}$, $6p_{1/2}$, and $6p_{3/2}$. The hole and particle states can be combined to give 12 odd-parity states with J=1. These states are listed in Table I, where both jj and LS designations are given. Note that LS labeling is used in all of the references mentioned previously [9–15], even though the LS-coupling description is most appropriate for low stages of ionization. For simplicity, we replace the $4d_j^{-1}nl_{j'}$ or $4d^{-1}nl$ designations

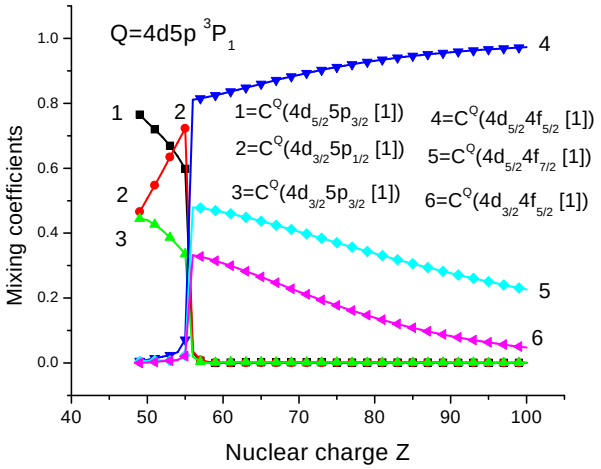

FIG. 2: Mixing coefficients as functions of Z for odd-parity states with J=1 in Pd-like ions.

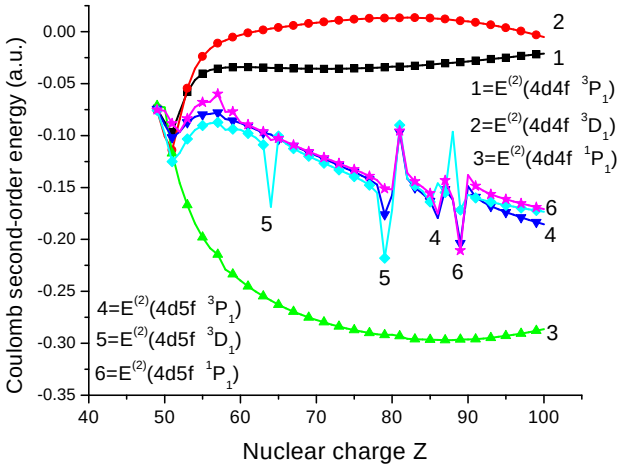

FIG. 3: Second-order Coulomb energies as functions of Z for $4d4f$ and $4d5f$ states with J=1 in Pd-like ions.

by $4d_jnl_{j'}$ or $4dnl$ in Table I and in all of the following tables and text.

We have already mentioned that there is strong mixing between $4d4f$ and $4d5p$ states. In Fig. 2, we illustrate the contribution of these states to the $4d5p\,^3P_1$ level in interval Z=49-100. For Z=49-53, the largest contribution to the $4d5p\,^3P_1$ level is from the $4d_{5/2}5p_{3/2}[1]$ state. The $4d_{3/2}5p_{1/2}[1]$ state dominates for Z = 54–55 and, for Z > 56, the $4d_{5/2}4f_{5/2}[1]$ state contributes about 90% to the $4d5p\,^3P_1$ level. The same strong mixing affects $4d5p\,^1P_1$ and $4d5p\,^3D_1$ levels. From Fig. 2 it is obvious that the LS labeling $4d4p\,^3P_1$ given in Table I is meaningful only for low stages of ionization; starting from Z=58 the dominant contribution to this state is from the $4d_{5/2}5f_{5/2}\,[1]$ configuration.

B. Z dependence of energies in Pd-like ions

In Fig. 3, we illustrate the Z-dependence of the second-order energy corrections $E^{(2)}$ for $4d4f\,^3P_1$, $^3D_1$, $^1P_1$ and $4d5f\,^3P_1$, $^3D_1$, $^1P_1$ states in Pd-like ions. The second-order energy $E^{(2)}$ is a smooth function of Z for $4d4f$ and $4d5p$ configurations, but exhibits a few sharp features for $4d5f$ configurations. These very strong irregularities occur for the $4d5f\,^3P_1$ state (Z=81, 89), $4d5f\,^3D_1$ state (Z=64, 79, 81, 88), and $4d5f\,^1P_1$ state (Z=81, 89) and are explained by vanishing energy denominators in MBPT expressions for correlation corrections. We give some numerical details relevant to this issue in Appendix C.

Energies of the J=1 $4d4f$ and $4d5p$ states relative to the ground state are shown in Fig. 4. We plot the six energy levels within the odd-parity J=1 complex that are involved in the mixing of states illustrated in Fig. 2.

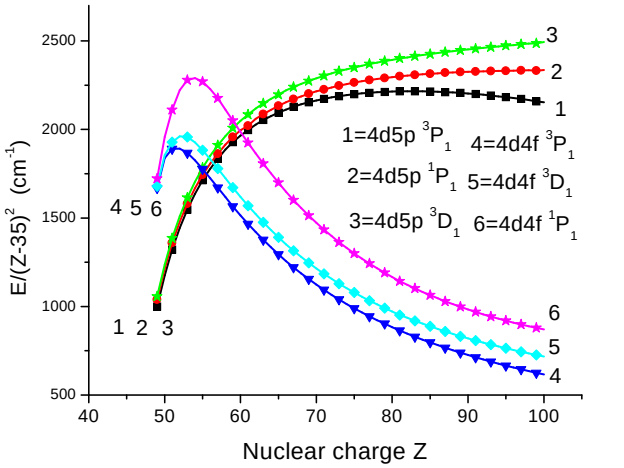

FIG. 4: Excitation energies $(E/(Z-35)^2)$ in cm^{-1} for $4d4f$ and $4d5p$ states with J=1 as functions of Z.

It was already shown that the largest mixing coefficient contributing to the $4d5p\,^3P_1$ level is different for $Z \leq 54$ and $Z \geq$55. This change can also be observed in Fig. 4. The first ($4d5p\,^3P_1$) and fourth ($4d4f\,^3P_1$) level curves cross for Z=55. The difference $E[4d5p\,^3P_1]-E[4d4f\,^3P_1]$ at Z=55 is just 4% of the energy $E[4d5p\,^3P_1]$. A similar Z dependence and strong mixing for these levels was found by Sugar and Kaufman [9].

III. THIRD-ORDER MBPT CONTRIBUTION TO ENERGIES OF PD-LIKE IONS

The importance of third-order contributions in obtaining precise energies for Li-, Na-, Cu- and Ag-like ions was established in Refs. [19–22]. Moreover, large third-order contributions for $4f_{5/2}$ and $4f_{7/2}$ states in Ce IV and Pr V were found recently in Ref. [23] where third-order energies for $4f$ states were found to be about 35% of second-order energies.

Results of the present third-order calculations for energies of $4f$ and $5p$ particle states, which are evaluated as described in Ref. [22], are shown in Fig. 5, where we compare second- and third-order contributions. We compare $E^{(3)}$ and $E^{(2)}$ for $4d$ hole states in Fig. 6. We see from these figures that $E^{(3)}$ and $E^{(2)}$ have different signs; consequently, third-order contributions substantially decrease the magnitude of the correlation correction. Values of $E^{(3)}(4f)$ and $E^{(3)}(5p)$ slowly increase with increasing Z, whereas the value of $E^{(3)}(4d)$ decreases with increasing Z.

We include both one- and two-body contributions to the second-order energy, but only one-body contribution to the third-order energy in the present work. Indeed, we find that the two-body contribution to $E^{(2)}$ is smaller in magnitude than the one-body contribution by a factor of 2–5. In Fig. 7, the second-order energy is compared to the combined second- and third-order energy. The data presented in Fig. 7 are obtained by diagonalizing the energy matrix within the $4d4f$ model space. Differences between second-order values and second-order + third-order values are seen to be almost constant and equal to 0.03 - 0.04 a.u..

Results of our relativistic many-body perturbation theory in second- and third-order MBPT (labeled MBPT2 and MBPT3) are given in Table II. In this table, we compare our results for energy levels of the three hole-particle $4d4f$ states of interest in Pd-like ions with experimental measurements performed in Refs. [9–11, 13]. Although our results are generally in good agreement with experimental data, discrepancies were found. One cause for these discrepancies is the omission of two-body third-order correlation corrections. However, we have no explanation for the increasing discrepancy found in the $4d4f\,^1P_1$ level with the increasing Z; 680 cm^{-1} for Z=65, 1400 cm^{-1} for Z=66, and 17900cm^{-1} for Z=78.

IV. ELECTRIC-DIPOLE MATRIX ELEMENTS

In the following paragraphs, we present electric-dipole (E1) matrix elements for transitions between the odd-parity J=1 states belonging to the $4d_j4f_{j'}[1]$, $4d_j5f_{j'}[1]$, $4d_j5p_{1/2}[1]$, and $4d_j6p_{j'}[1]$ configurations and the ground state for Pd-like ions. Analytical expressions for E1 matrix elements in second-order MBPT are given in Ref. [6] and will not be repeated here. The first- and second-order Coulomb Breit corrections to E1 matrix elements are referred to as $Z^{(1)}$, $Z^{(2)}$, and $B^{(2)}$, respectively, in the text below. These contributions are calculated in both length and velocity forms, and include contributions from negative energy states.

V. OSCILLATOR STRENGTHS, TRANSITION RATES, AND LINE STRENGTHS

Oscillator strengths for the twelve E1 lines from ($4d4f\ ^3P_1, ^3D_1, ^1P_1$), ($4d5f\ ^3P_1, ^3D_1, ^1P_1$), ($4d5p\ ^3P_1, ^1P_1, ^3D_1$) and ($4d6p\ ^3P_1, ^1P_1, ^3D_1$) levels to the ground state are plotted in Fig. 8. The sharp features in the curves shown in these figures are explained in many cases by strong mixing of states inside of the odd-parity complex with J=1.

The deep minimum in the curves labeled $4d4f\,^3P_1$, (Z=88), $4d5f\,^3P_1$, (Z=92), and $4d5p\,^3P_1$ (Z=56) are due to mixing of the $[4d_{5/2}4f_{5/2}\ [1] + 4d_{5/2}4f_{7/2}\ [1]]$, $[4d_{5/2}5f_{5/2}\ [1] + 4d_{5/2}5f_{7/2}\ [1]]$, and $[4d_{3/2}5p_{1/2}\ [1] + 4d_{5/2}5p_{3/2}\ [1]]$ states, respectively. It should be noted that the mixing of those states is not very large (about 15-20%) in the first two cases; however, the ratios of dipole-matrix elements, $Z^{(1+2)}(0 - 4d_{5/2}4f_{7/2}\ [1])$ and $Z^{(1+2)}(0 - 4d_{5/2}4f_{5/2}\ [1])$ as well as matrix elements, $Z^{(1+2)}(0 - 4d_{5/2}5f_{7/2}\ [1])$ and $Z^{(1+2)}(0 - 4d_{5/2}5f_{5/2}\ [1])$ are equal to 4-5 (see Table VIII) and the sign of these ratios is different from the sign of the corresponding ratio of mixing coefficients. This leads to cancellation since the coupled matrix elements are a product of matrix elements and mixing coefficients. As a result, deep minima occur in the curves $4d4f\,^3P_1$ at Z=88 and $4d5f\,^3P_1$ at Z=92.

Singularities in the curves labeled $4d6p\,^3P_1$, $^1P_1\,^3D_1$ have a different origin. We found a sharp increase in the second-order RPA contributions for Z=57 ($4d_{3/2}6p_{1/2}$) and for Z=61, 67, and 79 ($4d_{5/2}6p_{3/2}$) resulting from very small the energy denominators. As a result, the second-order contribution becomes very large, leading to deviations from the smooth curves in Fig. 8. Details are given in Appendix D.

In Table III, we compare our MBPT values of E1 transition rates with theoretical results of Biémont [8]. We list results for transitions between $4d4f$ and $4d5p$ excited states and the ground state for selected ions (Z= 92, 90, 80, and 70). The differences between our results and those from Ref. [8] range from 0 - 10% for $4d5p\,^3P_1$, $^1P_1$ levels and 30 - 40% for $4d4f\,^3P_1$, $^3D_1$, $^1P_1$ and $4d5p\,^3D_1$ levels. These differences are the result of the different computational methods used; the present results are from second-order MBPT calculations while results in Ref. [8] were obtained in the MCDF approximation. Second-order contributions to matrix elements, which are relatively large, are illustrated for Xe^{+8} in Table IX of Appendix B where we compare first- and second-order MBPT values. The fact that correlation corrections to matrix elements in Pd-like ions are large was also noted in [7].

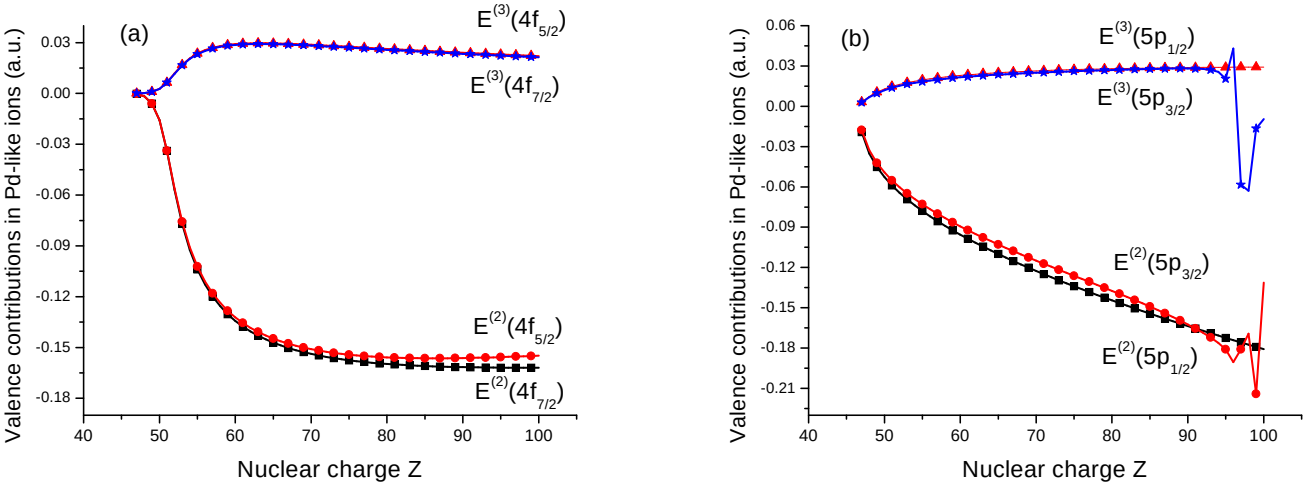

FIG. 5: Second- and third-order particle contributions to energies in Pd-like ions.

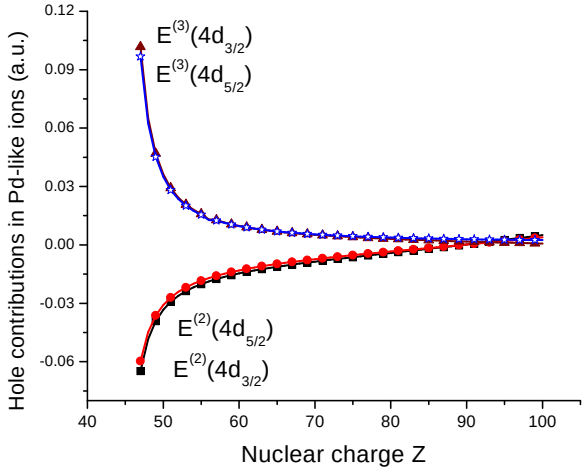

FIG. 6: Second- and third-order hole contributions to energies in Pd-like ions.

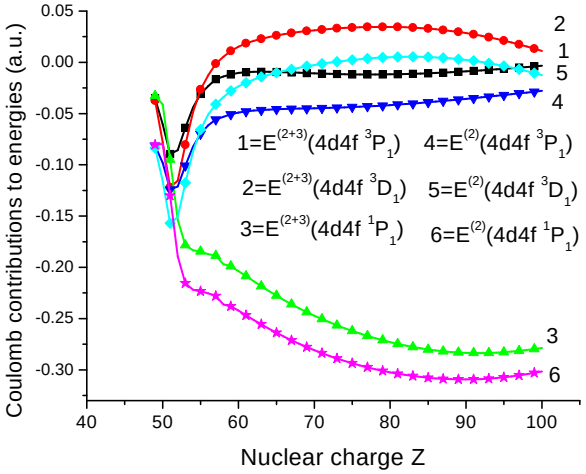

FIG. 7: Coulomb contributions to the energies as functions of Z for $4d4f$ states with J=1 in Pd-like ions.

In Table IV, we compare our MBPT results for line strengths $S^{(1)}$ and $S^{(1+2)}$ with theoretical results $S_{\rm HF}$ and $S_{\rm MBPT}$ from Younger [7]. In particular, we list results for the transition between $4d4f\ ^1P_1$ excited state and the ground state for nine ions from $Z = 50$ to Z=74 presented in Ref. [7]. It should be noted that the results for nine ions in [7] were obtained only in the HF approximation $S_{\rm HF}$. The MBPT results in [7] were given only for three ions, Z= 54, 60, and 74. Our MBPT results, $S^{(1+2)}$ and those from [7] $S_{\rm MBPT}$ agree surprisingly well (1%, and 2% for ions with Z= 60, and 74, respectively.

VI. CONCLUSION

In summary, a systematic second-order MBPT study of excitation energies of the 12 $4d^{-1}4f$, $4d^{-1}5p$, $4d^{-1}5f$, and $4d^{-1}6p$ hole-particle states of Pd-like ions has been presented. Theoretical excitation energies of Pd-like ions In^{3+}–Pt^{32+} differ from existing experimental wavelengths data at the level of 0.01% -2.0%.

We also presented a systematic second-order relativistic MBPT study of reduced matrix elements, line strengths, oscillator strengths, and transition rates for electric-dipole transitions into the ground state in Pd-like ions with nuclear charges ranging from Z = 49 to

TABLE II: Excitation energies (in cm^{-1}) for $4d4f$ states in Pd-like ions calculated in MBPT2 and MBPT3 approximation. Comparison with experimental measurements performed in Ref. [11] -*a*, Ref. [13] -*b*, Ref. [9] -*c*, and Ref. [10] -*d*.

Ion	$^3P_1$	$^3D_1$	$^1P_1$	$^3P_1$	$^3D_1$	$^1P_1$	$^3P_1$	$^3D_1$	$^1P_1$
	Z=49				Z=50			Z=51	
MBPT2	329175	330205	338330	417464	419175	440551	488162	492090	538076
MBPT3	339295	340331	348834	425733	427500	449023	495775	499774	545783
expt.	328552[a]	333968[a]	343006[a]	412316[a]	423372[a]	446348[a]	485458[a]	502840[a]	547063[a]
	Z=52				Z=53			Z=54	
MBPT2	548489	560104	636538	605122	626451	734487	659075	688918	825331
MBPT3	556247	567918	644346	613232	634606	742624	667463	697343	833731
expt.	550113[a]	573155[a]	649003[a]	609143[a]	636983[a]	744596[a]	665450[b]	696310[b]	832410[b]
	Z=55				Z=56			Z=57	
MBPT2	710670	747434	907529	760405	802939	982632	808685	856225	1052467
MBPT3	719227	756021	916089	768786	811345	991010	817330	864890	1061104
expt.	716673[a]	752513[a]	912500[a]		806445[c]	986280[c]		856201[c]	1055253[c]
	Z=58				Z=59			Z=60	
MBPT2	855552	907801	1117388	901636	958429	1180977	946988	1008024	1241899
MBPT3	864167	916432	1125991	910195	966999	1189519	955472	1016514	1250362
expt		909512[c]	1120610[c]		959462[c]	1183540[c]		1008580[c]	1242950[c]
	Z=61				Z=62			Z=63	
MBPT2	991684	1056908	1301162	1035830	1105244	1359173	1079511	1153158	1416226
MBPT3	1000090	1065315	1309544	1044130	1113540	1367445	1087710	1161348	1424393
expt.					1105100[c]	1361200[c]	1096700[c]	1152800	1420370[c]
	Z=64				Z=65			Z=66	
MBPT2	1122793	1200753	1472547	1165730	1248112	1528313	1208368	1295305	1583669
MBPT3	1130887	1208834	1480606	1173718	1256082	1536262	1216249	1303164	1591509
expt.		1200200[c]	1478500[c]	1183500[c]	1246900[c]	1535580[c]		1294600[c]	1592900[c]
	Z=67				Z=68			Z=69	
MBPT2	1250745	1342393	1638735	1292892	1389426	1693611	1334839	1436454	1748384
MBPT3	1258520	1350141	1646465	1300563	1397065	1701232	1342407	1443984	1755897
expt.			1649500[c]		1388100[d]	1706200[d]			
	Z=70				Z=71			Z=72	
MBPT2	1376609	1483514	1803129	1418222	1530645	1857916	1459699	1577880	1912804
MBPT3	1384076	1490938	1810537	1425590	1537965	1865220	1466970	1585097	1920007
expt.			1818300[d]						1930400[d]
	Z=73				Z=74			Z=75	
MBPT2	1501053	1625249	1967851	1542300	1672779	2023109	1583452	1720497	2078627
MBPT3	1508229	1632365	1974954	1549385	1679798	2030115	1590447	1727420	2085537
expt.					1670800	2043000			
	Z=76				Z=77			Z=78	
MBPT2	1624521	1768425	2134452	1665517	1816587	2190629	1706448	1865001	2247202
MBPT3	1631428	1775255	2141269	1672339	1823326	2197355	1713187	1871651	2253839
expt.									2271700

100. The reduced dipole matrix elements include correlation corrections from Coulomb and Breit interactions. Both length and velocity forms of the matrix elements were evaluated, and small differences, caused by the nonlocality of the starting DHF potential, were found between the two forms. Second-order MBPT transition energies were used to evaluate oscillator strengths and transition rates. We believe that our results will be useful in analyzing existing experimental data and in planning new experiments.

Acknowledgments

The work of W.R.J. was supported in part by National Science Foundation Grant No. PHY-01-39928. The work of U.I.S. was supported by DOE/NNSA under UNR grant DE-FC52-01NV14050. U.I.S. would like to thank M.S. Safronova for helpful discussions.

APPENDIX A: ENERGY MATRIX FOR XE^{+8}

In Table V, we list contributions to the second-order energies for the special case of Pd-like xenon, $Z = 54$. In the table, we give the one-body and two-body second-order Coulomb contributions to the energy matrix la-

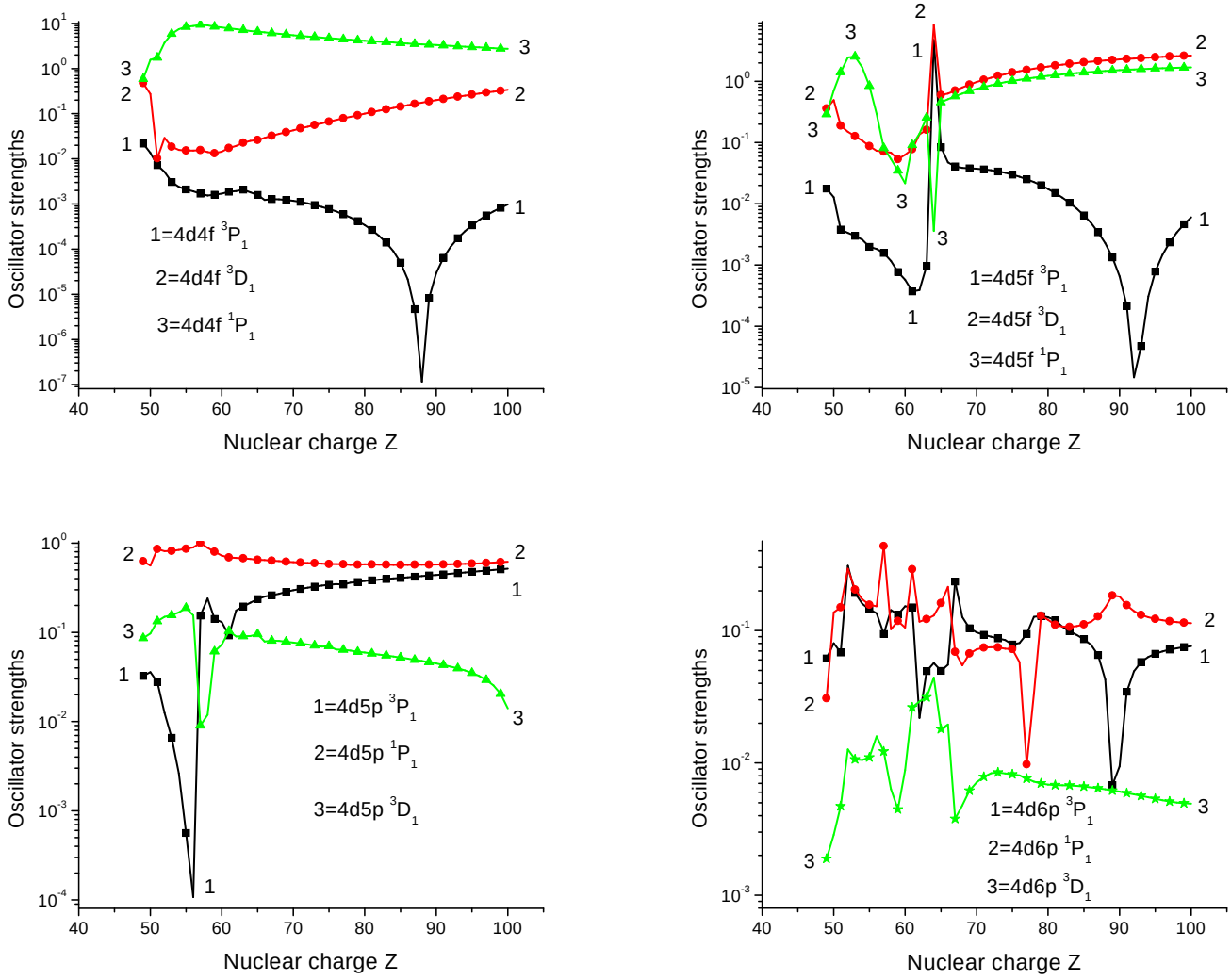

FIG. 8: Oscillator strengths for transitions between the ground state and $4d4f$, $4d5f$, $4d5p$, and $4d6p$ states as functions of Z.

beled $E_1^{(2)}$ and $E_2^{(2)}$, respectively. The corresponding Breit-Coulomb contributions are listed in columns headed $B_1^{(2)}$ and $B_2^{(2)}$. The one-body second-order energy is a sum of the valence and hole energies; the later being the dominant contribution [6]. The values of $E_1^{(2)}$ and $B_1^{(2)}$ are non-zero only for diagonal matrix elements. There are 12 diagonal and 60 non-diagonal matrix elements for $4d_jnl_{j'}$ [1] hole-particle states but we list only a small subset of the non-diagonal matrix elements in Table V. The second-order Breit-Coulomb corrections are relatively large and, therefore, must be included in accurate calculations. The non-diagonal matrix elements listed in the columns headed $E_2^{(2)}$ and $B_2^{(2)}$ are comparable with diagonal two-body matrix elements. However, the one-body contributions, $E_1^{(2)}$ and $B_1^{(2)}$, are larger than the corresponding two-body contributions, $E_2^{(2)}$ and $B_2^{(2)}$. As a result, the net second-order diagonal matrix elements are larger than the non-diagonal matrix elements in Table VI.

In Table VI, we present results for Coulomb contributions, $E^{(0)}$, $E^{(1)}$, and $E^{(2)}$, and Breit-Coulomb corrections, $B^{(1)}$ and $B^{(2)}$ obtained before diagonalization. Corrections for the frequency-dependence of the Breit interaction [24] are included in the first order only. The difference between first-order Breit-Coulomb corrections calculated with and without frequency dependence is less than 1%. As one sees from Table VI, the ratio of non-diagonal and diagonal matrix elements is larger for first-order contributions than for second-order contributions. Another difference in first- and second-order contributions is symmetry properties: first-order non-diagonal matrix elements are symmetric while the second-order non-diagonal matrix elements are not. $E^{(2)}(a'v'[J], av[J])$ and $E^{(2)}(av[J], a'v'[J])$ differ in some cases by factors of 2–3 and occasionally have opposite

TABLE III: Transition rates (A_r in s^{-1}) in Pd-like ions for transitions between excited $4d4f\,^3P_1$, $^3D_1$, $^1P_1$, $4d5p\,^3P_1$, $^1P_1$, $^3D_1$, states and the ground state. Comparison of the present MBPT results (a) with theoretical results from Biémont [8] (b).

Level		Z=92	Z=90	Z=80	Z=70
$4d4f\,^3P_1$	(a)	1.30[08]	3.18[07]	2.43[08]	5.02[08]
$4d4f\,^3D_1$	(a)	3.31[11]	2.70[11]	8.54[10]	2.10[10]
	(b)	4.47[11]	3.66[11]	1.18[11]	2.92[10]
$4d4f\,^1P_1$	(a)	7.11[12]	6.80[12]	5.41[12]	4.24[12]
	(b)	9.47[12]	9.09[12]	7.32[12]	5.74[12]
$4d5p\,^3P_1$	(a)	5.16[12]	4.37[12]	1.70[12]	4.68[11]
	(b)	5.50[12]	4.66[12]	1.81[12]	5.01[11]
$4d5p\,^1P_1$	(a)	7.42[12]	6.37[12]	2.80[12]	1.01[12]
	(b)	6.75[12]	5.87[12]	2.69[12]	1.01[12]
$4d5p\,^3D_1$	(a)	5.91[11]	5.50[11]	3.12[11]	1.36[11]
	(b)	7.78[11]	6.90[11]	3.54[11]	1.28[11]

TABLE IV: Line strengths (S in a.u.) in Pd-like ions for transitions between excited $4d4f\,^1P_1$ states and the ground state. Comparison of our first-order $S^{(1)}$ and second-order $S^{(1+2)}$ line strengths with theoretical results (a) from Younger [7].

Ion	$S^{(1)}$	$S^{(1+2)}$	$S^a_{\rm HF}$	$S^a_{\rm MBPT}$
Sn VII	1.611	1.129	1.445	
Te VII	3.167	1.843	2.599	
I VIII	3.574	2.504	3.180	
Xe IX	3.803	2.853	3.579	2.36
Cs X	3.804	2.920	3.701	
Ba XI	3.648	2.803	3.593	
Nd XV	2.683	2.063	2.606	2.079
Ho XXII	1.575	1.182	1.514	
W XXIX	1.022	0.766	0.9834	0.7512

signs.

To determine the first-order energies of the states under consideration, we diagonalize the symmetric first-order effective Hamiltonian, including both the Coulomb and Breit interactions. The first-order expansion coefficient $C^N(av[J])$ is the N-th eigenvector of the first-order effective Hamiltonian and $E^{(1)}[N]$ is the corresponding eigenvalue. The resulting eigenvectors are used to evaluate the second-order Coulomb correction $E^{(2)}[N]$ as well as the second-order Breit-Coulomb correction $B^{(2)}[N]$.

In Table VII, we list the following contributions to the energies of 15 excited states in Xe^{+8}: the sum of the zeroth and first-order energies $E^{(0+1)} = E^{(0)} + E^{(1)} + B^{(1)}_{hf}$, the second-order Coulomb energy $E^{(2)}$, the second-order Breit-Coulomb correction $B^{(2)}$, and the sum of the above contributions $E_{\rm tot}$.

APPENDIX B: E1 MATRIX ELEMENTS FOR XE^{+8}

In Table VIII, we list values of *uncoupled* first- and second-order E1 matrix elements $Z^{(1)}$, $Z^{(2)}$, $B^{(2)}$, together with derivative terms $P^{(\rm derv)}$ for the twelve E1 transitions between odd-parity J=1 states with and the ground state in Pd-like xenon, Z=54. Matrix elements are given in both length (L) and velocity (V) forms. We see that the first-order matrix elements, $Z^{(1)}_L$ and $Z^{(1)}_V$, differ by 20–30% and the L–V differences between second-order matrix elements are much larger for some transitions. The large differences in first plus second order matrix elements disappear after coupling.

Values of *coupled* E1 matrix elements in length and velocity forms are given in Table IX for the transitions considered in Table VIII. The first two columns in Table IX show L and V values of reduced matrix elements calculated in first order. The $L-V$ difference is about 20–25%. Including second-order contributions (columns headed MBPT in Table IX) decreases the $L-V$ difference to 3-4%. This large $L-V$ difference in the lowest-order calculation arises because we start our MBPT calculations using a non-local DHF potential. If we were to replace the DHF potential by a local potential, the differences would disappear completely. It should be emphasized that we include negative energy state (NES) contributions to sums over intermediate states (see Ref. [17] for details). Neglecting the NES contributions leads to small changes in the L-form matrix elements but to substantial changes in some of the V-form matrix elements with a consequent loss of form independence.

APPENDIX C: THE SECOND-ORDER HOLE-PARTICLE CONTRIBUTION

To understand the irregularities in Fig. 3, we consider the second-order hole-particle contribution to the valence energy $E^{(2)}_v$ (Eq.(2.6) in Ref.[6]) and to the interaction energy $E^{R_3}(a'v'[J], av[J])$ (Eq.(2.10) in Ref.[6]). A typical double-excitation contribution to the valence energy has the form [6]

$$A(v) \propto \sum_{mnc} \sum_{l} \frac{X_l(vcmn) X_l(mncv)}{\epsilon_v + \epsilon_c - \epsilon_m - \epsilon_n}\,, \qquad \text{(C1)}$$

where $X_l(vwmn)$ is the product of a Slater integral and angular momentum coefficients, ϵ_m and ϵ_n are zeroth-order one-particle energies, ϵ_c is a zeroth-order core orbital energy, and ϵ_v is the zeroth-order valence orbital energy.

We found a sharp increase in values of the second-order valence energy for $5f_{7/2}$ states (Z=79) and $5f_{5/2}$ states (Z=89). The denominator of one term in Eq. (C1) $\epsilon_{5f_{7/2}} + \epsilon_{4d_{5/2}} - \epsilon_{5s_{1/2}} - \epsilon_{4f_{5/2}}$ = -0.0076 occurs for Z = 79. Moreover, the denominator of another term

TABLE V: Second-order contributions to energy matrices (a.u.) for odd-parity states with J=1 in Pd-like xenon, Z = 54. One-body and two-body second-order Coulomb and Breit-Coulomb contributions are given in columns labeled $E_1^{(2)}$, $E_2^{(2)}$, $B_1^{(2)}$, and $B_2^{(2)}$, respectively.

$4d_1j_1\ nl_2j_2$	$4l_3j_3\ n'l_4j_4$	$E_1^{(2)}$	$E_2^{(2)}$	$B_1^{(2)}$	$B_2^{(2)}$
		$4d_j4f_{j'}[1]$+$4d_j5f_{j'}[1]$ states			
$4d_{5/2}4f_{5/2}$	$4d_{5/2}4f_{5/2}$	-0.112309	0.073927	0.007163	0.000856
$4d_{5/2}4f_{7/2}$	$4d_{5/2}4f_{7/2}$	-0.110820	-0.024173	0.007267	0.000255
$4d_{3/2}4f_{5/2}$	$4d_{3/2}4f_{5/2}$	-0.114133	0.006638	0.007272	0.000509
$4d_{5/2}5f_{5/2}$	$4d_{5/2}5f_{5/2}$	-0.054365	-0.032374	0.010636	0.000140
$4d_{5/2}5f_{7/2}$	$4d_{5/2}5f_{7/2}$	-0.054092	-0.017309	0.010650	0.000085
$4d_{3/2}5f_{5/2}$	$4d_{3/2}5f_{5/2}$	-0.056189	-0.020837	0.010745	0.000144
$4d_{5/2}4f_{7/2}$	$4d_{3/2}4f_{5/2}$	0	0.086037	0	0.000462
$4d_{3/2}4f_{5/2}$	$4d_{5/2}4f_{7/2}$	0	0.086871	0	0.000441
$4d_{5/2}4f_{5/2}$	$4d_{5/2}5f_{7/2}$	0	0.022362	0	0.000307
$4d_{5/2}5f_{7/2}$	$4d_{5/2}4f_{5/2}$	0	-0.040251	0	-0.000422
		$4d_j5p_{j'}[1]$+$4d_j6p_{j'}[1]$ states			
$4d_{3/2}5p_{3/2}$	$4d_{3/2}5p_{3/2}$	-0.090867	0.023576	0.010131	0.000597
$4d_{3/2}5p_{1/2}$	$4d_{3/2}5p_{1/2}$	-0.095575	0.025054	0.010004	0.000727
$4d_{5/2}5p_{3/2}$	$4d_{5/2}5p_{3/2}$	-0.089043	0.022102	0.010022	0.000531
$4d_{3/2}6p_{3/2}$	$4d_{3/2}6p_{3/2}$	-0.048985	-0.012761	0.011453	0.000256
$4d_{3/2}6p_{1/2}$	$4d_{3/2}6p_{1/2}$	-0.050015	-0.008980	0.011427	0.000323
$4d_{5/2}6p_{3/2}$	$4d_{5/2}6p_{3/2}$	-0.047160	-0.010888	0.011345	0.000235
$4d_{3/2}5p_{3/2}$	$4d_{3/2}6p_{3/2}$	0	0.008101	0	0.000037
$4d_{3/2}6p_{3/2}$	$4d_{3/2}5p_{3/2}$	0	-0.000260	0	0.000491
$4d_{5/2}6p_{3/2}$	$4d_{3/2}5p_{3/2}$	0	-0.004177	0	0.000085
$4d_{3/2}5p_{1/2}$	$4d_{5/2}5p_{3/2}$	0	0.000672	0	0.000050

$\epsilon_{5f_{5/2}} + \epsilon_{4d_{3/2}} - \epsilon_{4f_{7/2}} - \epsilon_{5s_{1/2}}$ = -0.0099 occurs for Z = 89. These small denominators lead to the increases in $A(5f_{7/2})$ and $A(5f_{5/2})$ by factors 3-5, leading in turn to sharp deviations from smooth curves in Fig. 3 for Z=79 and Z=89.

Two terms in $E^{R_3}(a'v'[J], av[J])$ are responsible for sharp features in the curves shown in Fig. 3 for Z=64 and Z=81. The first term is [6]

$$E_1^{R_3}(a'v'[J], av[J]) \propto \sum_{nc} \frac{Z_J(vcan)Z_J(a'nv'c)}{\epsilon_v + \epsilon_c - \epsilon_n - \epsilon_a}\,, \quad \text{(C2)}$$

where $Z_J(vcan)$ is a symmetrized Coulomb integral (see Ref.[6]). We found an increase (by a factor of 2) in the contribution from (C2) for Z=64. In this case, the denominator is $\epsilon_{5f_{7/2}} + \epsilon_{4p_{3/2}} - \epsilon_{5s_{1/2}} - \epsilon_{4d_{5/2}}$ = -0.00746, leading to the sharp feature at Z=64 in Fig. 3 The second term is [6]

$$E_2^{R_3}(a'v'[J], av[J]) \propto \sum_{nc} \frac{Z_J(vcv'n)Z_J(a'nac)}{\epsilon_v + \epsilon_c - \epsilon_n - \epsilon_{v'}}\,. \quad \text{(C3)}$$

We also found a factor 2 increase in the contribution from (C3) for Z=81. In this case, the denominator is $\epsilon_{5f_{7/2}} + \epsilon_{4p_{3/2}} - \epsilon_{4f_{7/2}} - \epsilon_{4f_{7/2}}$ = 0.0069, leading to the sharp feature in Fig. 3 at Z=81.

APPENDIX D: THE SECOND-ORDER DIPOLE MATRIX ELEMENT

A typical contribution from one of the second-order reduced matrix elements $Z_1^{(RPA)}[0 - av[1]]$ has the form [6]

$$Z_1^{(\mathrm{RPA})}(0 - av[1]) \propto \sum_{b,i} \frac{Z_1(bi)Z_1(aivb)}{\varepsilon_b + \varepsilon_v - \varepsilon_i - \varepsilon_a} \quad \text{(D1)}$$

The one-electron electric-dipole matrix element $Z_1(bi)$, defined in Ref. [17] includes retardation and is calculated in length and velocity forms. In the sum over i, only terms with vanishing denominators are excluded. We found the sharp increase (by a factor of 2-5) in values of the $Z_1^{(\mathrm{RPA})}(0 - av[1])$ contributions for Z=57 (av=$4d_{3/2}6p_{1/2}$) and for Z=61, 67, and 79 (av=$4d_{5/2}6p_{3/2}$) by resulting from very small values of the denominator D in Eq. (D1).

(i) av=$4d_{3/2}6p_{1/2}$, Z=57:
$D = \epsilon_{4d_{5/2}} + \epsilon_{6p_{1/2}} - \epsilon_{5f_{7/2}} - \epsilon_{4d_{3/2}}$ =
- 10.1802 - 3.1639 + 3.0443 + 10.2988 = -0.0010.

(ii) av=$4d_{5/2}6p_{3/2}$, Z=61:
$D = \epsilon_{4p_{3/2}} + \epsilon_{6p_{3/2}} - \epsilon_{5s_{1/2}} - \epsilon_{4d_{5/2}}$ =
- 20.4963 - 5.2512 + 9.8620 + 15.8751 = -0.0104.

(iii) av=$4d_{5/2}6p_{3/2}$, Z=67:
$D = \epsilon_{4p_{1/2}} + \epsilon_{6p_{3/2}} - \epsilon_{5s_{1/2}} - \epsilon_{4d_{5/2}}$ =
- 33.8633 - 9.3802 + 16.8595 + 26.3713 = -0.0127.

(iiii) av=$4d_{5/2}6p_{3/2}$, Z=79:

TABLE VI: Diagonal and non-diagonal contributions to the energy matrix (a.u.). These contributions are listed for a odd-parity hole-particle states with J=1 in Pd-like xenon, $Z = 54$.

		$E^{(0)}$	$E^{(1)}$	$B^{(1)}_{hf}$	$E^{(2)}$	$B^{(2)}$
		$4d_j4f_{j'}[1]$+$4d_j5f_{j'}[1]$ states				
$4d_{5/2}4f_{5/2}$	$4d_{5/2}4f_{5/2}$	4.002727	-0.851736	-0.005658	-0.038381	0.008019
$4d_{5/2}4f_{7/2}$	$4d_{5/2}4f_{7/2}$	4.004396	-0.411782	-0.006227	-0.134993	0.007522
$4d_{3/2}4f_{5/2}$	$4d_{3/2}4f_{5/2}$	4.082366	-0.535663	-0.008069	-0.107495	0.007781
$4d_{5/2}5f_{5/2}$	$4d_{5/2}5f_{5/2}$	5.011411	-0.441221	-0.006660	-0.086739	0.010777
$4d_{5/2}5f_{7/2}$	$4d_{5/2}5f_{7/2}$	5.010231	-0.352094	-0.006814	-0.071401	0.010734
$4d_{3/2}5f_{5/2}$	$4d_{3/2}5f_{5/2}$	5.091050	-0.375533	-0.008909	-0.077026	0.010889
$4d_{5/2}4f_{7/2}$	$4d_{3/2}4f_{5/2}$	0	-0.390363	0.000198	0.086037	0.000462
$4d_{3/2}4f_{5/2}$	$4d_{5/2}4f_{7/2}$	0	-0.390363	0.000198	0.086871	0.000441
$4d_{5/2}4f_{5/2}$	$4d_{5/2}5f_{5/2}$	0	0.196436	-0.000054	-0.020582	0.000553
$4d_{5/2}5f_{5/2}$	$4d_{5/2}4f_{5/2}$	0	0.196436	-0.000054	0.000836	-0.001032
		$4d_j5p_{j'}[1]$+$4d_j6p_{j'}[1]$ states				
$4d_{3/2}5p_{3/2}$	$4d_{3/2}5p_{3/2}$	3.465775	-0.606582	-0.006781	-0.067291	0.010728
$4d_{3/2}5p_{1/2}$	$4d_{3/2}5p_{1/2}$	3.383917	-0.591982	-0.005648	-0.070521	0.010731
$4d_{5/2}5p_{3/2}$	$4d_{5/2}5p_{3/2}$	3.386136	-0.588964	-0.004578	-0.066941	0.010553
$4d_{3/2}6p_{3/2}$	$4d_{3/2}6p_{3/2}$	4.870283	-0.369668	-0.008334	-0.061745	0.011710
$4d_{3/2}6p_{1/2}$	$4d_{3/2}6p_{1/2}$	4.836995	-0.366928	-0.007893	-0.058995	0.011750
$4d_{5/2}6p_{3/2}$	$4d_{5/2}6p_{3/2}$	4.790643	-0.365499	-0.006115	-0.058048	0.011580
$4d_{3/2}5p_{3/2}$	$4d_{3/2}6p_{3/2}$	0	-0.122309	0.000006	0.008101	0.000037
$4d_{3/2}6p_{3/2}$	$4d_{3/2}5p_{3/2}$	0	-0.122309	0.000006	-0.000260	0.000491
$4d_{5/2}6p_{3/2}$	$4d_{3/2}5p_{3/2}$	0	0.013930	0.000007	-0.004177	0.000085
$4d_{3/2}5p_{1/2}$	$4d_{5/2}5p_{3/2}$	0	-0.016847	0.000038	0.000672	0.000050

TABLE VII: Energies (cm^{-1}) of odd-parity states with J=1 relative to the ground state in the case of Pd-like xenon, $Z = 54$. $E^{(0+1)} \equiv E^{(0)} + E^{(1)} + B^{(1)}$

Level-jj	Level-LS	$E^{(0+1)}$	$E^{(2)}$	$B^{(2)}$	$E_{\rm tot}$
$4d_{5/2}4f_{5/2}$	$4d4f\,^3P_1$	667834	-10251	1775	659358
$4d_{5/2}4f_{7/2}$	$4d4f\,^3D_1$	701081	-7805	1799	695075
$4d_{3/2}4f_{5/2}$	$4d4f\,^1P_1$	865559	-40484	1633	826708
$4d_{5/2}5f_{5/2}$	$4d5f\,^3P_1$	1005954	-17983	2338	990309
$4d_{5/2}5f_{7/2}$	$4d5f\,^3D_1$	1016961	-20794	2340	998506
$4d_{3/2}5f_{5/2}$	$4d5f\,^1P_1$	1052759	-15939	2344	1039164
$4d_{3/2}5p_{3/2}$	$4d5p\,^3P_1$	603083	-14790	2352	590645
$4d_{3/2}5p_{1/2}$	$4d5p\,^1P_1$	614480	-15022	2333	601792
$4d_{5/2}5p_{3/2}$	$4d5p\,^3D_1$	627641	-14591	2368	615418
$4d_{3/2}6p_{3/2}$	$4d6p\,^3P_1$	971260	-12843	2534	960950
$4d_{3/2}6p_{1/2}$	$4d6p\,^1P_1$	980603	-13000	2568	970171
$4d_{5/2}6p_{3/2}$	$4d6p\,^3D_1$	988529	-13931	2561	977159

$$D = \epsilon_{4p_{3/2}} + \epsilon_{6p_{3/2}} - \epsilon_{5d_{5/2}} - \epsilon_{4d_{5/2}} =$$
$$- 62.6012 - 20.8374 + 29.1876 + 54.2837 = 0.0327.$$

[1] E. Avgoustoglou, W. R. Johnson, D. R. Plante, J. Sapirstein, S. Sheinerman, and S. A. Blundell, Phys. Rev. A **46**, 5478 (1992).

[2] E. Avgoustoglou, W. R. Johnson, and J. Sapirstein, Phys. Rev. A **51**, 1196 (1195).

[3] E. Avgoustoglou and Z. W. Liu, Phys. Rev. A **54**, 1351 (1996).

[4] E. N. Avgoustoglou and D. R. Beck, Phys. Rev. A **57**, 4286 (1998).

[5] U. I. Safronova, C. Namba, I. Murakami, W. R. Johnson, and M. Safronova, Phys. Rev. A **64**, 012517 (2001).

[6] U. I. Safronova, W. R. Johnson, and J. Albritton, Phys. Rev. A **62**, 052505 (2000).

[7] S. M. Younger, Phys. Rev. A **22**, 2682 (1980).

[8] E. Biémont, J. Phys. B **30**, 4207 (1997).

[9] J. Sugar and V. Kaufman, Phys. Scr. **26**, 419 (1982).

[10] J. Sugar and V. Kaufman, J. Opt. Soc. Am. B **10**, 799 (1993).

[11] S. S. Churilov, Y. N. Joshi, and A. N. Ryabtsev, J. Phys. B **27**, 5485 (1994).

TABLE VIII: Uncoupled reduced matrix elements in length L and velocity V forms for transitions from odd-parity states with $J = 1$ into the ground state in Xe^{+8}.

$av[J]$	$Z_L^{(1)}$	$Z_V^{(1)}$	$Z_L^{(2)}$	$Z_V^{(2)}$	$B_L^{(2)}$	$B_V^{(2)}$	$P_L^{(\mathrm{derv})}$	$P_V^{(\mathrm{derv})}$
$4d_{5/2}4f_{5/2}[1]$	-0.355034	-0.276197	0.046114	-0.023046	-0.000152	0.000407	-0.355039	-0.000125
$4d_{5/2}4f_{7/2}[1]$	1.587063	1.236167	-0.215121	0.094093	0.001007	-0.001359	1.586495	-0.000624
$4d_{3/2}4f_{5/2}[1]$	1.311071	1.024024	-0.181366	0.074495	0.001042	-0.001473	1.310734	-0.000241
$4d_{5/2}5f_{5/2}[1]$	-0.084623	-0.063932	0.016209	-0.007417	-0.000108	0.000059	-0.084661	-0.000053
$4d_{5/2}5f_{7/2}[1]$	0.381899	0.289004	-0.073331	0.032624	0.000189	-0.000396	0.381889	-0.000119
$4d_{3/2}5f_{5/2}[1]$	0.323203	0.245750	-0.062910	0.026535	0.000361	-0.000330	0.323232	-0.000017
$4d_{3/2}5p_{3/2}[1]$	-0.602369	-0.459228	0.031482	-0.003936	-0.000571	0.000312	-0.602254	-0.000063
$4d_{3/2}5p_{1/2}[1]$	0.471485	0.360397	-0.072135	-0.035844	0.000278	-0.000523	0.471361	-0.000033
$4d_{5/2}5p_{3/2}[1]$	-0.192146	-0.147879	0.004731	-0.004808	-0.000226	0.000154	-0.192062	0.000069
$4d_{3/2}6p_{3/2}[1]$	-0.214308	-0.167094	-0.074938	-0.073807	0.000059	0.000359	-0.214288	-0.000049
$4d_{3/2}6p_{1/2}[1]$	-0.163207	-0.127896	-0.059201	-0.057414	-0.000052	0.000263	-0.163176	0.000002
$4d_{5/2}6p_{3/2}[1]$	-0.069267	-0.054494	-0.021644	-0.021551	-0.000065	0.000072	-0.069237	0.000029

TABLE IX: Coupled reduced matrix elements in length L and velocity V forms for transitions from odd-parity states with $J = 1$ to the ground state in Xe^{+8}.

	First order		First + Second order	
$av[J]$	L	V	L	V
$4d4f\,^3P_1$	-0.040259	-0.030620	-0.034381	-0.033315
$4d4f\,^3D_1$	0.094469	0.071445	0.086029	0.082300
$4d4f\,^1P_1$	1.950059	1.522731	1.689214	1.649958
$4d5f\,^3P_1$	0.034392	0.026473	0.029157	0.027995
$4d5f\,^3D_1$	-0.221525	-0.169910	-0.186553	-0.179215
$4d5f\,^1P_1$	0.870436	0.668357	0.727942	0.701366
$4d5p\,^3P_1$	-0.001250	0.000244	-0.037850	-0.028815
$4d5p\,^1P_1$	0.748234	0.571264	0.670136	0.676280
$4d5p\,^3D_1$	-0.293622	-0.225074	-0.296226	-0.291124
$4d6p\,^3P_1$	-0.159274	-0.124664	-0.232483	-0.213014
$4d6p\,^1P_1$	0.161649	0.127249	0.240488	0.220414
$4d6p\,^3D_1$	-0.043139	-0.034031	-0.059278	-0.054801

[12] S. S. Churilov, V. A. Azarov, A. N. Ryabtsev, W. -Ü. L. Tchang-Brillet, and J. -F. Wyart, Phys. Scr. **61**, 420 (2000).

[13] S. S. Churilov, A. N. Ryabtsev, W. -Ü. L. Tchang-Brillet, and J. -F. Wyart, Phys. Scr. **65**, 40 (2002).

[14] S. S. Churilov and Y. N. Joshi, Phys. Scr. T **100**, 98 (2002).

[15] S. Churilov, Y. N. Joshi, and J. Reader, Opt. Lett. **28**, 1478 (2003).

[16] M. S. Safronova, W. R. Johnson, and U. I. Safronova, Phys. Rev. A **53**, 4036 (1996).

[17] U. I. Safronova, W. R. Johnson, M. S. Safronova, and A. Derevianko, Phys. Scr. **59**, 286 (1999).

[18] W. R. Johnson, S. A. Blundell, and J. Sapirstein, Phys. Rev. A **37**, 2764 (1988).

[19] W. R. Johnson, S. A. Blundell, and J. Sapirstein, Phys. Rev. A **37**, 2794 (1988).

[20] W. R. Johnson, S. A. Blundell, and J. Sapirstein, Phys. Rev. A **38**, 2699 (1988).

[21] W. R. Johnson, S. A. Blundell, and J. Sapirstein, Phys. Rev. A **42**, 1087 (1990).

[22] U. I. Safronova, I. M. Savukov, M. S. Safronova, and W. R. Johnson, Phys. Rev. A **68**, 062505 (2003).

[23] I. M. Savukov, W. R. Johnson, U. I. Safronova, and M. S. Safronova, Phys. Rev. A **67**, 042504 (2003).

[24] M. H. Chen, K. T. Cheng, and W. R. Johnson, Phys. Rev. A **47**, 3692 (1993).